Development of a cancer cells self-activating and miR-125a-5p expressing poly-pharmacological nanodrug for cancer treatment

YUNG-CHIEH CHANG[1*], MIN-CHIEH SHIEH[2*], YEN-HSUAN CHANG[3], WEI-LUN HUANG[4,5],
WU-CHOU SU[4,6], FONG-YU CHENG[7] and CHUN HEI ANTONIO CHEUNG[1,3]

[1]Institute of Basic Medical Sciences, College of Medicine, National Cheng Kung University, Tainan 701401;
[2]Division of General Surgery, Department of Surgery, Ditmanson Medical Foundation Chia-Yi Christian Hospital,
Chiayi 600566; [3]Department of Pharmacology, College of Medicine, [4]Center of Applied Nanomedicine,
[5]Department of Medical Laboratory Science and Biotechnology, National Cheng Kung University; [6]Department of Oncology,
College of Medicine and Hospital, National Cheng Kung University, Tainan 701401; [7]Department of Chemistry,
College of Sciences, Chinese Culture University, Taipei 111396, Taiwan, R.O.C.

Abstract. Cancer cells can acquire resistance to targeted therapeutic agents when the designated targets or their downstream signaling molecules develop protein conformational or activity changes. There is an increasing interest in developing poly-pharmacologic anticancer agents to target multiple oncoproteins or signaling pathways in cancer cells. The microRNA 125a-5p (miR-125a-5p) is a tumor suppressor, and its expression has frequently been downregulated in tumors. By contrast, the anti-apoptotic molecule BIRC5/SURVIVIN is highly expressed in tumors but not in the differentiated normal tissues. In the present study, the development of a *BIRC5* gene promoter-driven, miR-125a-5p expressing, poly-L-lysine-conjugated magnetite iron poly-pharmacologic nanodrug (pL-MNP-pSur-125a) was reported. The cancer cells self-activating property and the anticancer effects of this nanodrug were examined in both the multidrug efflux protein ABCB1/MDR1-expressing/-non-expressing cancer cells *in vitro* and *in vivo*. It was demonstrated that pL-MNP-pSur-125a decreased the expression of ERBB2/HER2, HDAC5, BIRC5, and SP1, which are hot therapeutic targets for cancer *in vitro*.

Notably, pL-MNP-pSur-125a also downregulated the expression of TDO2 in the human KB cervical carcinoma cells. PL-MNP-pSur-125a decreased the viability of various *BIRC5*-expressing cancer cells, regardless of the tissue origin or the expression of ABCB1, but not of the human *BIRC5*-non-expressing HMEC-1 endothelial cells. *In vivo*, pL-MNP-pSur-125a exhibited potent antitumor growth effects, but without inducing liver toxicity, in various zebrafish human-ABCB1-expressing and ABCB1-non-expressing tumor xenograft models. In conclusion, pL-MNP-pSur-125a is an easy-to-prepare and a promising poly-pharmacological anticancer nanodrug that has the potential to manage numerous malignancies, particularly for patients with BIRC5/ABCB1-related drug resistance after prolonged chemotherapeutic treatments.

Correspondence to: Dr Chun Hei Antonio Cheung, Department of Pharmacology, College of Medicine, National Cheng Kung University, 1 University Road, Tainan 701401, Taiwan, R.O.C.
E-mail: acheung@mail.ncku.edu.tw

Dr Fong-Yu Cheng, Department of Chemistry, College of Sciences, Chinese Culture University, 55 Huagang Road, Taipei 111396, Taiwan, R.O.C.
E-mail: zfy3@ulive.pccu.edu.tw

*Contributed equally

Introduction

Numerous targeted therapeutic agents have been developed for cancer treatment in the past two decades. For example, the anti-Erb-B2 receptor tyrosine kinase 2 (ERBB2/HER2) monoclonal antibody Trastuzumab (Herceptin), is commonly used nowadays for treating patients with ERBB2+ (HER2+) breast tumor. On the other hand, the epidermal growth factor receptor (EGFR) inhibitor Gefitinib (Iressa), is used to manage patients with advanced non-small cell lung cancer, which is often EGFR+. Despite the early success of various targeted therapeutics, drug resistance remains a major problem in clinical practice. As cancer cells can acquire resistance to targeted therapeutic agents when the designated-targets or their downstream signaling molecules develop protein conformational or activity changes due to gene mutations or amplifications, agents specificity targeting a single molecule or pathway often fails particularly in patients after prolonged treatment (1). This leads to the recent interest in poly-pharmacology, which refers to the design or use of pharmacological agents that act on multiple targets or disease pathways (2,3).

The microRNA (miR)-125a-5p is a recently discovered tumor suppressor. In clinical situations, low expression levels of miR-125a-5p were associated with enhanced malignant potential and poor prognosis in patients with head and neck, gastric, and breast cancer (4-6). At the cellular level, ectopic overexpression of miR-125a-5p inhibits the proliferation (or promotes apoptosis), migration, invasion, and epithelial-mesenchymal transition (EMT) of breast, colorectal and lung cancer cells (7-12). Ectopic overexpression of miR-125a-5p also restores the sensitivity to cisplatin in the cisplatin-resistant cervical cancer cells and counteracts EGF-induced cell proliferation and invasion in cervical cancer cells (13,14). At the molecular level, miR-125a-5p negatively regulates the expression of ERBB2, baculoviral IAP repeat containing 5 (BIRC5/SURVIVIN), Sp1 transcription factor (SP1), LIM kinase 1 (LIMK1), and polypeptide N-acetylgalactosaminyltransferase 7 (GALNT7) in cells, in which upregulation of these molecules is known to promote tumorigenesis, tumor metastasis and drug resistance (4,6,14-18).

BIRC5 is a member of the inhibitor of apoptosis proteins (IAPs) family known for its inhibitory effects on caspase activity. Physiologically, BIRC5 plays an important role in brain development during embryogenesis (19). Unlike other IAPs, BIRC5 is highly expressed in different tumor types (Fig. S1A) but its expression remains low/undetectable in the differentiated normal and undamaged tissues (20-24). BIRC5 is also highly expressed in cancer stem cells (25,26). Clinically, high expression levels of BIRC5 is associated with poor prognosis in patients with cancer (Fig. S1B) (26,27). As upregulation of BIRC5 promotes tumorigenesis and tumor drug resistance, various efforts have been made in the development of the BIRC5-targeting anticancer therapies, including targeted therapy and vaccination (28-35). However, none of these BIRC5-targeting therapies has yet been approved by FDA for clinical application, mainly due to the lack of efficacy during clinical trials.

Polymeric gene delivery systems offer increased amounts of plasmid DNA uptake and the possibility of controlling the rate and conditions of release of plasmid DNA after administration. Plasmid DNA complexed with poly-L-lysine can be protected against digestion by nucleases present in the physiological environment (36). It was previously revealed that liposomal transfection of a *BIRC5* promoter-driven antisense *BIRC5*-expressing plasmid DNA (pSur/AS-Sur) induces apoptosis in *BIRC5*-expressing (BIRC5⁺) cancer cells but not in the *BIRC5* non-expressing (BIRC5⁻) human umbilical vein endothelial cells (HUVEC) *in vitro* (37). In the present study, the multi-molecules/pathways-targeting *BIRC5* promoter-driven *miR-125a-5p* expressing plasmid DNA (pSur-125a) loaded nanoparticles was created, in which the biodegradable and biocompatible poly-L-lysine polymer was used to encapsulate pSur-125a. The feasibility of using these nanoparticles to suppress the expression of various known miR-125a-5p-targeting cancer-related molecules such as ERBB2, SP1 and BIRC5 in BIRC5⁺ cancer cells was demonstrated. It was found that overexpression of miR-125a-5p downregulates the cellular expression of histone deacetylase 5 (HDAC5) and tryptophan 2,3-dioxygenase (TDO2), which is an enzyme that facilitates the production of kynurenine

and the related induction of immunosuppression in tumors. Overexpression of ATP Binding Cassette Subfamily B Member 1 (ABCB1/MDR1/P-gp) induces multidrug resistance in cancer cells. In the present study, it was also demonstrated that the anticancer efficacy and the molecular effects of these nanoparticles are not affected by the expression of ABCB1 in cancer cells *in vitro* and *in vivo*.

Materials and methods

Cell lines and cell culture conditions. Human KB (cervical carcinoma), MCF7 (breast adenocarcinoma), and MDA-MB-231 (breast adenocarcinoma) cells were originally obtained from the American Type Culture Collection. Human KB cells were cultured in RPMI-1640 medium (cat. no. 31800-022; Gibco; Thermo Fisher Scientific, Inc.) containing 5% fetal bovine serum (FBS) (cat. no. 04-001-1A; Biological Industries) and penicillin/streptomycin/glutamine (PSG). The human NTUB1 and the NTUB1-derived ABCB1-expressing NTU0.017 bladder carcinoma cells were kindly provided by Dr Jang-Yang Chang of Institute of Biotechnology and Pharmaceutical Research, National Health Research Institutes, Miaoli, Taiwan (38). Human NTUB1 and MDA-MB-231 cells were cultured in RPMI-1640 medium containing 10% FBS and PSG. The KB- and NTUB1-derived ABCB1-expressing, multidrug resistant KB-TAX50 and NTU0.017 cells were generated by the paclitaxel-driven selection and cultured in medium containing 50 and 17 nM paclitaxel, respectively, as previously described (37,39-41). Human MCF7 cells were cultured in α-MEM containing 5% FBS, PSG, and insulin-transferring-selenium supplement (ITS) (cat. no. 11074547001; Diagnostics). MCF7-TamC3 cells were created by prolonged culture of MCF7 cells under estrogen-depleted conditions. The cellular and molecular phenotypes of the MCF7-dervided estrogen-independent and tamoxifen-resistant MCF7-TamC3 breast cancer cells have already been characterized in previous studies (15,42). MCF7-TamC3 cells were cultured in phenol-red-free RPMI containing 5% charcoal-stripped FBS, PSG and ITS. The human HMEC-1 dermal microvascular endothelial cells were kindly provided by Dr Ben-Kuen Chen of the Department of Pharmacology of National Cheng Kung University, Taiwan. All cells were cultured at 37°C in a humidified incubator containing 5% CO_2 and were revealed to be mycoplasma free. The use of the aforementioned human cell lines in the present study was approved by the review board of Ministry of Science and Technology (Taiwan) and the biosafety committee of National Cheng Kung University (Taiwan).

Construction of the BIRC5 promoter driven miR-125a-5p expressing plasmid DNA. PCR was used to amplify the miR-125a-5p fragment and to insert the BspHI and EcoRI endonuclease restriction site on the 5' and 3' end of the PCR products (i.e. the newly synthesized miR-125a-5p fragments), respectively, with the use of the plasmid DNA pLV-[hsa-mir-125a] (cat. no. p087; BioSettia, Inc.) as template. The PCR cycle was carried out as follows: 98°C for 30 sec, followed up by 30 cycles of 98°C for 10 sec, 64.5°C for 30 sec, 72°C for 30 sec and then 72°C for 10 min using the following set of primers: forward, [designed to bind on the hsa-miR-125a

precursor sequence (miRNA accession no. MI0000469) carried by the plasmid DNA pLV-(hsa-mir-125a)] 5'-AA<u>TCAT GA</u>TCGAGGATCCTCGTTT-3' and reverse, 5'-AA<u>GAAT TC</u>GGTCAGGTTTCAGTTG-3'. The BspHI and EcoRI enzymatic sites are underlined. The PCR product was incubated with the restriction endonuclease BspHI and EcoRI to generate sticky ends. The destination vector pSur was created by incubating the plasmid DNA pDRIVE-hSurvivin (a vector that harbors a *BIRC5/survivin* gene promoter and a luciferase gene) (cat. no. pdrive-hsurvivin; InvivoGen) with BspHI and EcoRI for the removal of the luciferase gene. Then, the digested PCR product was ligated onto the linearized pSur in a molar ratio of 1:3. Successful ligation of the PCR product onto pSur (i.e. the creation of pSur-125a) was validated by DNA sequencing. The plasmid DNA pSur-125a was transformed into the DH5α *E. coli* cells for long term storage.

In vitro cell viability analysis. Cells (5,040 cells/well) were seeded onto each well of 96-well plates overnight before being transfected with the plasmid DNA for 48 h or treated with the nanoparticles for 96 h. After treatment, 200 μl of 3-(4,5-dimethylthiazol-2-yl)-2,5-diphenyltetrazolium bromide (MTT) solution (cat. no. 0793; diluted in phenol-red free RPMI in a ratio of 1:10; Amresco, LLC) was added to each well and incubated at 37°C for 4 h. Then, 100 μl MTT lysis buffer containing 500 ml/l dimethylformamide and 100 g/l sodium dodecyl sulfate, was added to each well and incubated for 16 h. Cell viability was quantified by measuring the absorbance of the solution at 570 nm using a SpectraMax® M5 microplate reader (Molecular Devices, LLC). The percentage of viable cells for each treatment group was calculated by adjusting the control group to 100%. Samples were assayed in duplicate and the experiments were repeated at least three times.

Wound healing (cell migration) assay. Cells (2.2x10⁴) were seeded onto each well of the culture inserts (Ibidi GmbH) for 24 h. Cell-free gaps (500 mm) were created after removing the culture inserts. Cells were treated with either pL-MNP-pSur-Emp or 0.5 x IC_{50} pL-MNP-pSur-125a. Images of the wound areas were captured by using an invert light microscope (CKX53; Olympus Corporation) after 9 h (NTU0.017 cells) or 12 h (NTUB1 cells). The average width of the wound was measured and analyzed using ImageJ 1.52a software (National Institutes of Health) to calculate the cell migration.

Transwell invasion (cell invasion) assay. The upper chambers of the Transwell plates with 8-μm pore size were coated with 20% Matrigel at 37°C for 1 h (BD Medical Technology). Cells (5x10⁵) were seeded onto the upper chamber of the Transwell (cat. no. 353182; Falcon; Corning Life Sciences) in serum-free culture medium containing indicated concentration of pL-MNP-pSur-Emp and pL-MNP-pSur-125a. Cell culture medium was added to the lower chamber containing the same concentration of pL-MNP-pSur-Emp and pL-MNP-pSur-125a as upper chamber. At 20 h post-treatment, cells attached on the revere side of the PET membrane were fixed with 4% paraformaldehyde solution at room temperature for 15 min and subsequently stained with 0.2% crystal violet solution at room temperature for 10 min. Images were captured by using

an invert microscope (OLYMPUS CKX53). The crystal violet was dissolved with 33% acetic acid, and the absorbance was measured (570 nm). The related invasion ability was calculated by comparing the absorbance intensity.

MicroRNA (miR-125a-5p) and BIRC5 mRNA expression analysis. Total RNAs were extracted using TRIzol® reagent (cat. no. 15596-026; Thermo Fisher Scientific, Inc.). To detect the expression level of miR-12a-5p in cells, complementary DNA (cDNA) was synthesized from the extracted RNA using TaqMan™ microRNA-specific primers, following protocol as described in the TaqMan® MicroRNA Reverse transcription kit (cat. no. 4427975; Thermo Fisher Scientific, Inc.). A TaqMan reverse transcription-quantitative PCR (RT-qPCR)-based microRNA assay (ID 002198-hsa-miR-125a-5p; ID 001093-RNU6B) was used to determine the expression of miR-125a-5p in cells. The target fragment was amplified according to the following protocol: preheating at 95°C for 10 min, 40 cycles at 95°C for 15 sec and 60°C for 1 min. The miRNA expression level was normalized with RNU6B, which was broadly used as the endogenous reference microRNA in different miRNA quantification studies. To detect the expression level of BIRC5 mRNA, total RNA was extracted using TRIzol® reagent and complementary DNA was synthesized from RNA using the RevertAid H Minus first strand cDNA synthesis kit (cat. no. K1631; Thermo Fisher Scientific, Inc.). The relative expression levels of BIRC5 and ACTA1 mRNA were determined by qPCR using primers as previously described (15). The specific primers with the following sequences were used in the present study: human BIRC5 forward, 5'-CTGCCTGGC AGCCCTTT-3' and reverse, 5'-CCTCCAAGAAGGGCCAGT TC-3'; human ACTA1 forward, 5'-GGCGGCACCACCATG TACCCT-3' and reverse, 5'-AGGGGCCGGACTCGTCAT ACT-3'. The target genes were quantified using the comparative threshold cycle (Ct) values $2^{-\Delta\Delta Cq}$ method (43) (ΔCq=Cq Target gene-CtRNU6B, $\Delta\Delta Cq$=ΔCq Treatment-ΔCq Control). Experiments were repeated thrice.

Western blot analysis. Cells were lysed using CelLytic™ M cell lysis reagent (cat. no. C2978; Sigma-Aldrich; Merck KGaA) containing 1 mM phenylmethylsulfonyl fluoride, 1 mM sodium fluoride and cocktail protease inhibitor cocktail (cat. no. 05892791001; Roche Diagnostics). The protein concentration was measured by the bicinchoninic acid (BCA) protein assay kit. Equal amounts of protein (30 μg) were subjected to sodium dodecyl-sulfate polyacrylamide gel electrophoresis (SDS-PAGE) on a 6, 10 or 12% acrylamide gel. The resolved proteins were transferred onto a PVDF membrane (cat. no. IPVH00010; Merck KGaA) and incubated with a blocking buffer TBST (5% non-fat dried milk in Tris-buffered saline with Tween-20 (cat. no. 9480; Calbiochem; Merck KGaA) for 1 h at room temperature before an overnight incubation at 4°C with the following primary antibodies: anti-cleaved CASP3 antibody (1:1,000; cat. no. 9664; Cell Signaling Technology, Inc.), anti-ERBB2 antibody (1:1,000; cat. no. UM570036; UltraMAB), anti-BIRC5 (Survivin) antibody (1:700; cat. no. AF886; R&D Systems, Inc.), anti-CDH1 (1:1,000; cat. no. 24E10; Cell Signaling Technology, Inc.), anti-HDAC5 antibody (1:1,000; cat. no. 161661-AP; ProteinTech Group, Inc.), anti-TDO2 (1:500; cat. no. GTX114831;

GeneTex, Inc.) anti-PARP antibody (1:1,000; cat. no. 9532; Cell Signaling Technology, Inc.), and anti-ACTA1 antibody (1:20,000; cat. no. MAB1501; Merck Millipore). The PVDF membrane was then washed thrice with TBS containing 0.1% Tween-20 before incubation for 1 h at room temperature with horseradish peroxidase-conjugated goat anti-rabbit antibodies (1:10,000; cat. no. AP132P; MilliporeSigma), mouse (1:10,000; cat. no. AP124P) or goat (1:10,000; cat. no. AP106P; both from MilliporeSigma) immunoglobulin G. Immunoreactive proteins were visualized using western blot enhanced chemiluminescence reagents (cat. no. WBKLS05000; Merck Millipore) and protein signals were detected by luminescence readers (FUJI LAS-100). The intensity of protein bands was determined by using the ImageJ 1.52a software (National Institutes of Health). Experiments were repeated at least three times.

Preparation of NH₂-Fe₃O₄ magnetic nanoparticles (MNPs). First, 1 M ferric chloride hexahydrate ($FeCl_3 \cdot 6H_2O$) and 2 M ferrous chloride tetrahydrate ($FeCl_2 \cdot 4H_2O$) were prepared by dissolving iron salts in 2 M hydrochloric acid (HCl) solution. Next, 4 ml of 1 M $FeCl_3$ solution and 1 ml 2 M $FeCl_2$ solution were mixed, and 1 ml of organic acid aqueous solution (0.5 g glycine dissolved in 1 ml deionized water) was then added to prepare the mixture solution. After vigorous stirring of the mixture solution, 5 M sodium hydroxide (NaOH) solution was then added drop by drop until the solution turned black. The solution was vigorously stirred again for 15 min at room temperature. Using a permanent magnet, the precipitated magnetic powder was fractionated, and the solution was subsequently discarded. Deionized water was then added to wash the precipitates thrice to remove excess salt. Subsequently, 3 g glycine, which was dissolved in 50 ml HCl, was added to the washed precipitates. The mixture solution was stirred for 5 min and then sonicated for 30 min. After adding deionized water and acetone in a volume ratio of Mixture solution: Deionized water: Acetone=5:2:3, the solution was centrifuged at 6,200 g for 10 min to discard the supernatant. Next, the following steps were repeated twice to remove excess organic acid in the suspension: 7 ml deionized water was added to dissolve and wash the precipitates, 3 ml acetone was added, and the mixture solution was centrifuged at 6,200 g for 10 min. In the end, NH_2-Fe_3O_4 MNPs were produced after the precipitates were dispersed in deionized water. An inductively coupled plasma analysis of the Fe ion concentration for the NH_2-Fe_3O_4 MNPs was measured by a spectro analyzer (Jobin-Yvon JY138).

Preparation of the plasmid DNA loaded poly-L-lysine-conjugated MNPs (pL-MNPs). The poly-L-lysine-conjugated MNPs (pL-MNPs) were prepared by mixing 5 ml of 0.1% (w/v) low molecular weight poly-L-lysine (MW 1,000 to 5,000; cat. no. P0879; Sigma-Aldrich; Merck KGaA) with 0.1 ml of 0.1 mM MNPs. After the mixture solution was stirred for 30 min at room temperature and centrifuged at 17,000 g for 10 min, the precipitates were isolated by removing the supernatant. The precipitates were then washed twice with deionized water. Finally, the precipitates (pL-MNPs) were dispersed and stored in deionized water. A total of 500 ng/µl of plasmid DNA (in aqueous solution) were incubated with 0.22 µM pL-MNPs. Next, deionized water and rhodamine 6G (R6G; final concentration, 10 µM) were added to the plasmid

DNA solution to achieve the final volume depending on the concentration of nanoparticles in the experiments. The volume ratio of 500 ng/µl of plasmid DNA:0.22 µM pL-MNP: deionized water=2:1:7. All samples were gently stirred at room temperature for at least 30 min before stirring at 4°C for 16 h.

Characterizations of the plasmid DNA-loaded pL-MNPs. Dynamic light scattering (DLS) was used to measure the size of plasmid DNA-loaded pL-MNPs, by Zetasizer Nano ZS90 (Malvern Instruments, Inc.). The zeta potential of pL-MNPs were determined by ELSZ-2000 (Otsuka Electronics Co., Ltd.). The surface morphology, shape and size of nanoparticles were measured by the scanning electron microscopy (SEM) at an accelerating voltage of 10 kV at a working distance of 9 mm. Samples prepared for SEM were firstly dropped on the cooper coin and collected after the solvent was evaporated at room temperature. Subsequently, samples were coated with gold for the sputter coating. Liquid transmission electron microscopy (liquid-TEM) was used for the *in situ* TEM image inspection for analyzing the structural and chemical properties, including size, structure and elements of plasmid DNA-loaded pL-MNPs. In the present study, the liquid-TEM was operated under the acceleration voltage of 200 kV (A JEOL JEM 2100 TEM).

DNase I protection assay. pSur-125a and PL-MNP- pSur-125a were incubated with DNase I at 37°C for 15, 30 min, 1 and 2 h in a final volume of 10 µl. The digestions were halted by incubating at 75°C for 10 min. The integrity of plasmid DNA was assessed by gel electrophoresis (0.8% agarose gel, 100 V), which was stained with the Healthview™ nucleic acid stain (cat. no. GN-NAS-100; Genomic).

In vitro plasmid DNA release assay. *In vitro* release of plasmid DNA from the plasmid DNA-loaded nanoparticle was performed in phosphate buffer saline (PBS) with different pH values (pH=7.4, 6, 5 and 4). 15 µg pL-MNP-pSur-Emp were incubated in 1 ml PBS with different pH value for various durations (1, 3, 6, 9, 12 and 24 h). After incubation, pL-MNP-pSur-Emp was stratified from the solution by using a magnet and the supernatant was collected to a new tube. The concentration of the plasmid DNA pSur-Emp in the supernatant was determined using spectrophotometry (MaestroGen, Inc.), and the total amount of the plasmid DNA presence was calculated using the following equation: Amount of plasmid DNA releasing (µg)=concentration of plasmid DNA (µg/µl) x 1,000 µl. The release percentage of plasmid DNA was determined using the following equation:

$$\% \text{ of releasing} = \frac{\text{Amount of plasmid DNA releasing } (\mu g)}{\text{Total amount of plasmid DNA loaded } (\mu g)} \times 100$$

In vivo drug potency evaluation. The animal protocol was approved (approval no. 109273) by the Institutional Animal Care and Use Committee (IACUC) of National Cheng Kung University (Tainan, Taiwan). Wild type zebrafish (*Danio rerio*, strain: AB) embryos were purchased from the Laboratory Animal Center, College of Medicine, National Cheng Kung University. Human KB, KB-TAX50 and MDA-MB-231 cancer cells were labeled with PKH67 to track tumor growth *in vivo*. Zebrafish embryos were anesthetized with 0.01% tricaine 48 h post-fertilization (hpf) and subsequently transplanted with

cancer cells. Total of 500 cancer cells were transplanted into the yolk sac of zebrafish embryos. A total of 1 h after cells transplantation, saline (negative control, N=24), pL-MNP-pSur-Emp (negative control, N=24), or pL-MNP-pSur-125a (N=24) were microinjected into yolk sac of zebrafish embryos. The saline or nanoparticles-treated zebrafish embryos were kept at 35˚C for 48 h. Tumor size was measured from images captured using fluorescence microscopy every 12 h post-treatment.

In vivo hepatotoxicity analysis. Zebrafish hepatotoxicity analysis was performed by the Taiwan zebrafish core facility of National Health Research Institute (NHRI). Briefly, 48 hpf transgenic zebrafish (fabp10a:mCherry) embryos were treated (i.e. microinjected) with saline (N=24), or the indicated concentrations of pL-MNP-pSur-Emp (N=24) and pL-MNP-pSur-125a (N=24) for 48 h. The size of liver was measured from images captured using fluorescence microscopy.

Statistical analysis. Each experiment was performed at least three times. Data are presented as the mean ± standard error of the mean. A two-tailed unpaired Student's t-test was used for comparisons between two groups. One-way ANOVA with Tukey's post hoc test were used for multi-group comparisons. All statistical analyses were performed using GraphPad Prism version 8 (GraphPad Software, Inc.). $P<0.05$ was considered to indicate a statistically significant difference.

Results

Transfection of pSur-125a decreases the viability of various BIRC5-expressing cancer cells. A *BIRC5* gene promoter driven *miR-125a-5p* expressing, multiple oncoproteins down-regulating, plasmid DNA (i.e. pSur-125a) was constructed. To confirm if pSur-125a functions as designed (Fig. 1A), the expression level of miR-125a-5p was examined in BIRC5^{+} cancer cells with or without liposomal delivery (i.e. transfection) of pSur-125a *in vitro*. The human KB and the KB-derived ABCB1-expressing, multidrug-resistant, KB-TAX50 cervical cancer cells (Fig. S2A) are known to express BIRC5 protein (37,39,44). Results of the qPCR analysis showed that transfection of pSur-125a significantly increased the amount of miR-125a-5p presence in both KB and KB-TAX50 cells compared with those transfected with pSur-Emp (i.e. the control plasmid DNA-*BIRC5* promoter containing, but without the miR-125a-5p insert) (Fig. 1B). YM155 is a small molecule BIRC5 inhibitor that suppresses BIRC5 protein expression at the transcriptional level through direct interactions with the *BIRC5* promoter region (45). In the present study, co-treatment with YM155 at a sub-lethal concentration (0.25 x IC$_{50}$ of cell viability) partially attenuated the expression effects of pSur-125a on miR-125a-5p in KB cells, confirming that the increased expression of miR-125a-5p was at least in part driven by the *BIRC5* promoter region located on pSur-125a (Fig. 1C). As revealed in Fig. 1D, transfection of pSur-125a decreased the expression of various known miR-125a-5p-targeting oncoproteins including ERBB2 and BIRC5 in KB and KB-TAX50 cancer cells. Transfection of pSur-125a also induced the protein cleavage of CASP3/caspase-3 and Poly (ADP-ribose) polymerase (PARP), which are markers for apoptosis,

confirming the pro-apoptotic property of pSur-125a in BIRC5^{+} cancer cells (Fig. 1D). It was previously demonstrated that HDAC5 downregulation increases miR-125a-5p expression in the human estrogen receptor-positive (ER[+]) MCF7 and the ER[+] MCF7-dervied estrogen-independent, tamoxifen resistant, MCF7-TamC3 breast cancer cells (15). Results of the western blot analysis showed that ectopic overexpression of miR-125a-5p decreased the expression of HDAC5 not only in KB and KB-TAX50, but also in MCF7, MCF7-TamC3 and MDA-MB-231 (triple-negative breast) cancer cells examined in the present study (Fig. 1E). These finding suggested that HDAC5 is a possible downstream affecting molecule of miR-125a-5p and a negative feedback loop possibly exists between HDAC5 and miR-125a-5p.

The viability of a panel of BIRC5^{+} cancer cells transfected with or without pSur-125a was examined (37,39,46). Results of the cell viability analysis revealed that transfection of pSur-125a significantly decreased the viability of KB, KB-TAX50, MCF7, MCF7-TamC3, MDA-MB-231, NTUB1 (bladder), and NTU0.017 (NTUB1-derived ABCB1-expressing) (Fig. S2A and B) cancer cells by 40-60% (Fig. 1F). In addition, the levels of effect of pSur-125a transfection on miR-125a-5p expression appear to be associated with the endogenous *BIRC5* gene transcription levels (by using amounts of *BIRC5* mRNA transcripts presence as an indicator) in the examined NTUB1, NTU0.017, and MDA-MB-231 cells (Fig. S2B and C). By contrast, transfection of pSur-125a did not affect the viability of the BIRC5-non-expressing (or only expressing at a relatively low level) human dermal microvascular endothelial HMEC-1 cells (Figs. S2D and 1F) and this result was unlikely caused by the limited transfection efficiency as bright green fluorescence signal could still be observed in HMEC-1 cells transfected with pCMV6-AC-GFP using the same plasmid DNA-liposome formulation (Fig. S2E).

Physicochemical characterizations of the pSur-125a-loaded poly-L-lysine-modified magnetic iron oxide nanoparticles (pL-MNP-pSur-125a). To increase the feasibility of utilizing pSur-125a as a therapeutic agent, the pSur-125a-loaded poly-L-lysine-modified magnetic iron oxide nanoparticles (pL-MNPs) (i.e. pL-MNP-pSur-125a) was developed. SEM images demonstrated that the pSur-Emp- and the pSur-125a-loaded nanoparticles (i.e. pL-MNP-pSur-Emp and pL-MNP-pSur-125a) were mostly in round shape under dehydrated conditions (Fig. 2A). The mean particle size of the nanoparticles pL-MNP (plasmid DNA-free), pL-MNP-pSur-Emp and pL-MNP-pSur-125a was ~289.1±9.5, 332.9±25.7 and 327.1±27.0 nm, respectively, as determined by the DLS analysis (Table I). The mean zeta (ζ) potential of pL-MNP, pL-MNP-pSur-Emp, and pLMNP-pSur-125a was +23.4±3.0, -45.0±4.3, and -39.8±3.4 mV, respectively (Table I). The chemical composition of pL-MNP-pSur-125a was determined by liquid TEM together with the energy dispersive X-ray spectroscopy (EDS) analysis. Images obtained by liquid TEM and results of the EDS analysis mapping together showed overlapping between the P element (representing the phosphate group of the DNA backbone) and the Fe element (representing the iron core of the nanoparticles), indicating successful loading of pSur-125a into the nanoparticles under the optimized conditions (Fig. 2B). The encapsulation
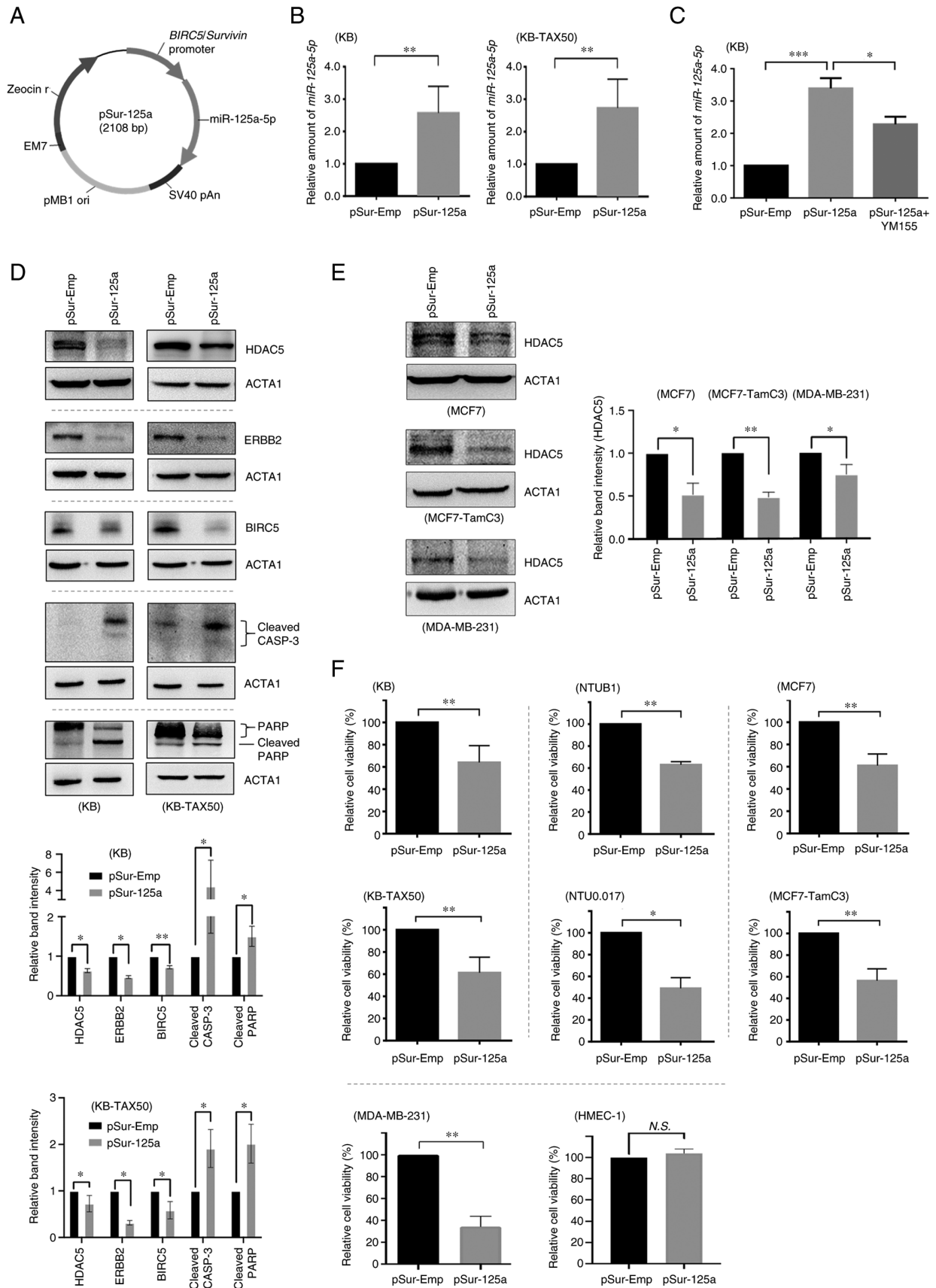
Figure 1. Transfection of pSur-125a downregulates the expression of various miR-125a-5p downstream targets and decreases the viability of both ABCB1-expressing/non-expressing cancer cells. (A) Schematic diagram showing the vector map of pSur-125a. (B) KB and KB-TAX50 cells were transfected with pSur-Emp or pSur-125a for 48 h. The relative amount of miR-125a-5p transcripts present in cells was determined by qPCR. (C) KB cells were transfected with pSur-Emp, pSur-125a, or pSur-125a co-treated with 2.55 nM YM155 for 48 h. The relative amount of miR-125a-5p transcripts present in cells was determined by qPCR. (D and E) Cancer cells were transfected with pSur-Emp or pSur-125a for 48 h. Expression of different proteins was determined by western blotting. ACTA1 was used as an internal control. (F) Cancer cells were transfected with pSur-Emp or pSur-125a for 48 h and the cell viability was determined using the MTT assay. *P<0.05, **P<0.01 and ***P<0.001. miR, microRNA; qPCR, quantitative PCR; N.S., no significance.
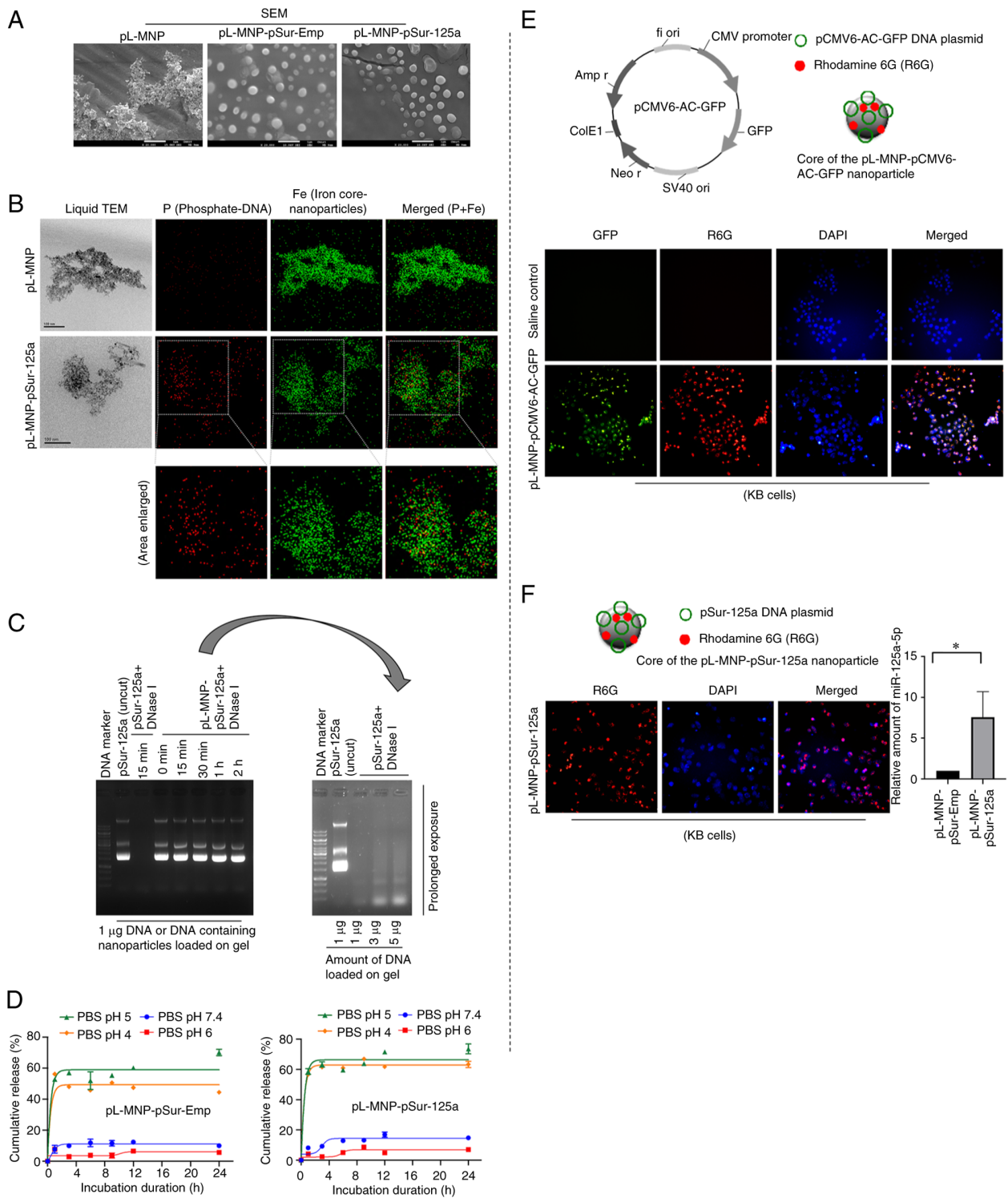
Figure 2. Physical and chemical characterizations of pL-MNP-pSur-Emp and pL-MNP-pSur-125a. (A) The shape and surface morphology of pL-MNP, pL-MNP-pSur-Emp, and pL-MNP-pSur-125a were determined by SEM. Scale bars: 1 μm. (B) Liquid TEM of pL-MNP and pL-MNP-pSur-125a and the corresponding EDS element mapping images showed the element compositions of pL-MNP and pL-MNP-pSur-125a (Red: phosphate; Green: iron). Scale bars: 100 nm. (C) Unencapsulated plasmid DNA pSur-125a and the nanoparticle pL-MNP-pSur-125a were incubated with or without DNase I for various durations. The integrity of DNA was examined by the DNase I protection assay. (D) pL-MNP-pSur-Emp and pL-MNP-pSur-125a were incubated in PBS with different pH value for indicated durations. Total amount of plasmid DNA released was measured with spectrophotometry. (E) KB cells were treated with pL-MNP-pCMV6-AC-GFP for 72 h. The uptake of pL-MNP-pCMV6-AC-GFP (red) and the expression of GFP (green) were visualized by fluorescence microscopy. Nucleus were counter-stained blue by DAPI. (F) KB cells were treated with pL-MNP-pSur-125a for 72 h. The uptake of pL-MNP-pSur-125a (red) was visualized by fluorescence microscopy. Nucleus were counterstained blue by DAPI. The relative amount of miR-125a-5p transcripts present in cells was determined by quantitative PCR. *P<0.05. SEM, scanning electron microscopy; TEM, transmission electron microscopy; miR, microRNA.

efficiency of pL-MNP-pSur-Emp and pL-MNP-pSur-125a was 42.6±3.2 and 45.8±2.8%, respectively. The loading capacity of pL-MNP-pSur-Emp and pL-MNP-pSur-125a was 59.6±4.5 and 64.1±3.9% (Table I).

Table I. Physicochemical properties of different nanoparticles.

Nanoparticles	pL-MNP	pL-MNP-pSur-Emp	pL-MNP-pSur-125a
Carried plasmid DNA	None	pSur-Emp	pSur-125a
Zeta potential (mV)	+23.4±3.0	-45.0±4.3	-39.8±3.4
Size (nm)	289.1±9.5	332.9±25.7	327.1±27.0
Encapsulation efficiency (%)	N/A	42.6±3.2	45.8±2.8
Loading capacity (%)	N/A	59.6±4.5	64.1±3.9

Circulating DNA and RNA are susceptible to degradation by nucleases in the body. As revealed in Fig. 2C, the DNase I protection assay results demonstrated that the plasmid DNA pSur-125a, which is encapsulated in our formulated pL-MNPs, remained intact in the presence of DNase I for up to 2 h incubation. By contrast, the naked plasmid DNA pSur-125a was completely digested by the same amount of DNase I within 15 min of incubation, suggesting that pL-MNPs could protect the encapsulated pSur-125a from nuclease digestion (Fig. 2C). The plasmid DNA pSur-125a needs to be released from the nanoparticles pL-MNP-pSur-125a within the targeted cancer cells before turning on its miR-125a-5p-expressing function. The *in vitro* plasmid DNA release assay showed that ~50-65% of the loaded plasmid DNAs (i.e. pSur-Emp and pSur-125a) were released in the medium at pH 4-5 (Fig. 2D). By contrast, only ~5-10% of the loaded plasmid DNAs were released in the medium at pH 6-7.4, suggesting the release of the plasmid DNAs is pH sensitive, and the loaded plasmid DNAs are likely to be released in the endo/lysosomal compartments of cells (Fig. 2D) (47). The plasmid DNA pCMV6-AC-GFP (a GFP-expressing construct) and R6G-containing nanoparticles (i.e. pL-MNP-pCMV6-AC-GFP) were created to confirm if the nanoparticles could penetrate and release the loaded plasmid DNAs in cells. These nanoparticles were synthesized using the same formulation and under the same conditions as for the production of pL-MNP-pSur-125a. Incorporating R6G in pL-MNP-pCMV6-AC-GFP enabled the tracing of these nanoparticles during the transfection process. To prevent the leaching of R6G from nanoparticles, R6G-isocyanate was covalently bonded to the amino groups of pL-MNP. Microscopic images demonstrated that most KB cells treated with pL-MNP-pCMV6-AC-GFP emitted both the red (i.e. R6G) and green (i.e. GFP) fluorescent signals, indicating that pL-MNP-pCMV6-AC-GFP nanoparticles are capable of penetrating the cells and releasing the loaded pCMV6-AC-GFP for ectopic expression of GFP (Fig. 2E). Similarly, fluorescence microscopy results revealed successful binding/penetration of pL-MNP-pSur-125a on/into KB cells (Fig. 2F). Of note, results of the qPCR analysis showed that the amount of the miR-125a-5p transcripts present in the pL-MNP-pSur-125a treated cells was significantly increased as compared with cells treated with the control nanoparticles pL-MNP-pSur-Emp, confirming that the plasmid DNA pSur-125a was successfully released by the nanoparticles and was also activated to express miR-125a-5p in the treated cells (Fig. 2F).

pL-MNP-pSur-125a exhibits the designated molecular and cellular functions in BIRC5-expressing cancer cells. At the molecular level and similar to the results of cells transfected with the plasmid DNA pSur-125a, KB cells treated with pL-MNP-pSur-125a also showed decreased protein expression levels of BIRC5, ERBB2, and HDAC5 (Fig. 3A). PL-MNP-pSur-125a also decreased the protein expression of HDAC5 in KB-TAX50 cells, confirming that HDAC5 is a downstream target of miR-125a-5p (Fig. S3A). By contrast, pL-MNP-pSur-125a increased the expression of CDH1/E-cadherin in KB cells, suggesting that the reduced expression of BIRC5, ERBB2 and HDAC5 protein was unlikely caused by the general reduction in the rate of protein synthesis in cells undergoing apoptosis and cell death (Fig. 3A). It was previously demonstrated that ectopic overexpression of miR-125a-5p decreases the expression of SP1, a transcription factor that is known to promote tumorigenesis upon upregulation in human SK-BR-3, MCF7, and MCF7-TamC3 breast cancer cells (15). In the present study, pL-MNP-pSur-125a decreased the expression of SP1 in KB cells, further confirming the poly-pharmacological effects (on various known miR-125a-5p-affecting molecules) of the nanodrug (Fig. 3A). Upregulation of tryptophan 2,3-dioxygenase (TDO2) promotes cancer immune evasion, and recently, TDO2 has been a hot therapeutic target for cancer (48,49). Intriguingly, it was found that pL-MNP-pSur-125a decreased the expression of TDO2 in KB but not in other examined cancer cells (Fig. S3B). To confirm if the downregulation of TDO2 was caused by miR-125a-5p overexpression, and not by the chemicals used for the nanoparticle production, cells were transfected with or without the plasmid DNA pSur-125a using liposomal reagents and the expression of TDO2 was examined. Similar to cells treated with pL-MNP-pSur-125a, transfection of pSur-125a also decreased the expression of TDO2 in KB cells (Fig. S3B). Collectively, these results suggested that miR-125a-5p differentially regulates TDO2 expression in different cancer cells.

The cellular effects of pL-MNP-pSur-125a were examined in both the BIRC5-expressing KB, KB-TAX50, NTUB1, NTU0.017 cancer cells and the BIRC5-non-expressing (or expressing at a relatively low level) HMEC-1 cells (50). In the present study, the cell viability assay results showed that pL-MNP-pSur-125a, but not pL-MNP-pSur-Emp, decreased the viability of KB, KB-TAX50, NTUB1 and NTU0.017 cells in a concentration-dependent manner (Fig. 3B). Importantly, pL-MNP-125a-5p is equally potent in inhibiting the growth of the multidrug resistance protein ABCB1 expressing (i.e. KB-TAX50 and NTU0.017) and their parental ABCB1 non-expressing (i.e. KB and NTUB1) cancer cells (Table II). Besides KB, NTUB1, and their derived ABCB1-expressing sublines, pL-MNP-pSur-125a
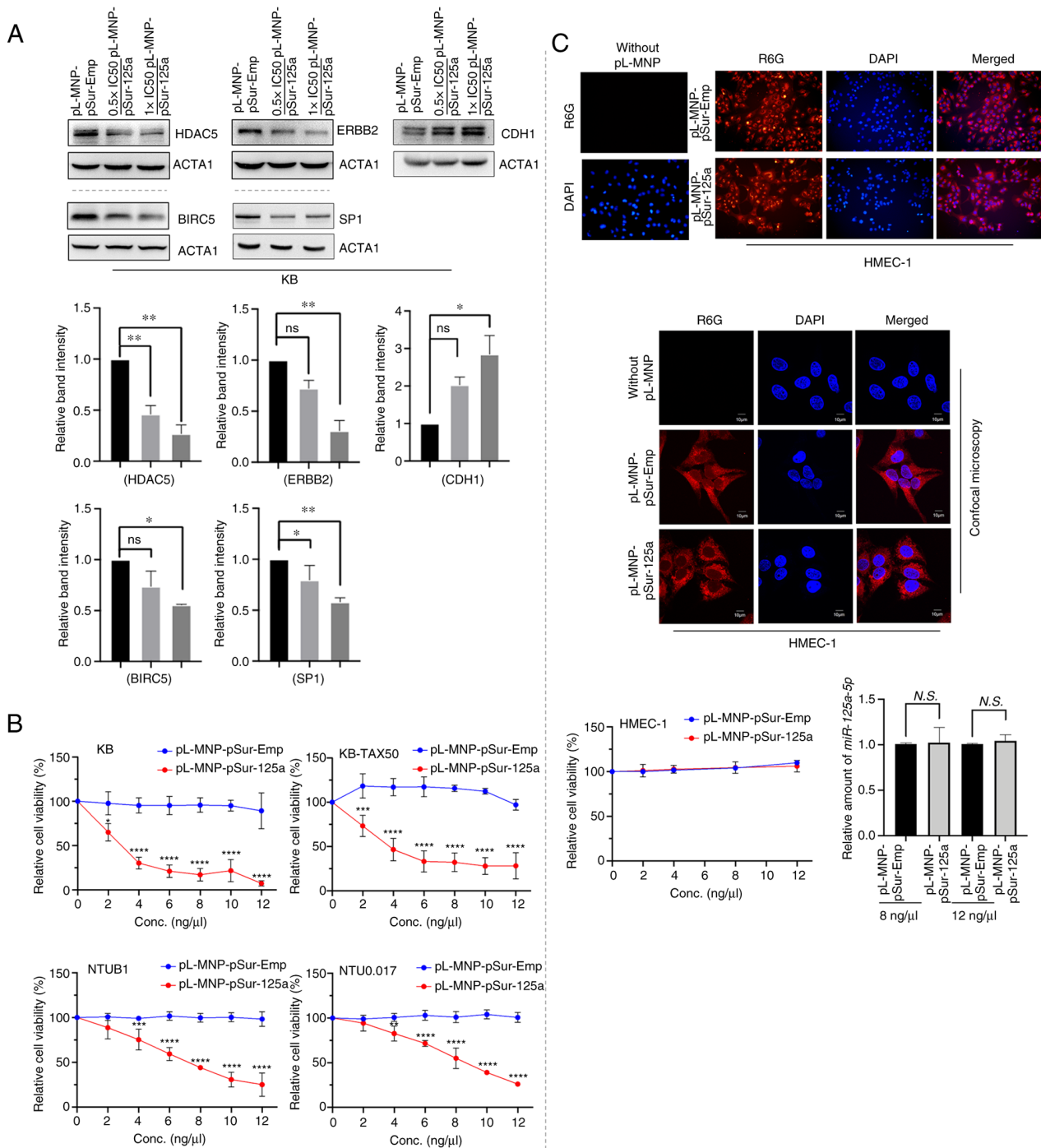
Figure 3. pL-MNP-pSur-125a is potent in targeting both ABCB1-expressing/non-expressing cancer cells. (A) KB cells were treated with either pL-MNP-pSur-Emp or pL-MNP-pSur-125a for 48 h. Expression of different proteins was determined by western blotting. ACTA1 was used as an internal control. (B) KB, KB-TAX50, NTUB1 and NTU0.017cells were treated with either pL-MNP-pSur-Emp or pL-MNP-pSur-125a for 96 h and the cell viability was determined using the MTT assay. (C) HMEC-1 cells were treated with either 8 ng/µl pL-MNP-pSur-Emp or pL-MNP-pSur-125a for 24 h (top and middle panels). Uptake of nanoparticles (Red) were visualized by fluorescence and confocal microscopy. Nucleus were counterstained blue by DAPI. HMEC-1 cells were treated with indicated concentrations of pL-MNP-pSur-Emp and pL-MNP-pSur-125a for 96 h (bottom left panel). Cell viability was determined using the MTT assay. The relative amount of miR-125a-5p transcripts present in cells was determined by quantitative PCR (bottom right panel). $^*P<0.05$, $^{**}P<0.01$, $^{***}P<0.001$ and $^{****}P<0.0001$.

(12 ng/µl, i.e. the maximum concentration used in the afore-mentioned cell viability assay) also decreased the viability (>50%) of various BIRC5^{+} cancer cell lines including MCF7, MCF7-TamC3, MDA-MB-231 and MIA-PaCa 2, as compared with those treated with pL-MNP-pSur-Emp (Fig. S3C). Of note, despite high levels of localization (and internalization) of the nanoparticles on cells, neither pL-MNP-pSur-Emp nor pL-MNP-pSur-125a exhibited any inhibitory effects on the viability of HMEC-1 cells *in vitro* (Fig. 3C). In addition, pL-MNP-pSur-125a, even at high concentrations (i.e. at 8 and 12 ng/µl), did not increase the expression of miR-125a-5p in HMEC-1 cells, further confirming that pL-MNP-pSur-125a is inactivated in BIRC5 non-expressing cells as designated (Fig. 3C).

Table II. pL-MNP-pSur-125a exhibits anti-proliferative activity against various types of cancer cells regardless of the expression of ABCB1.

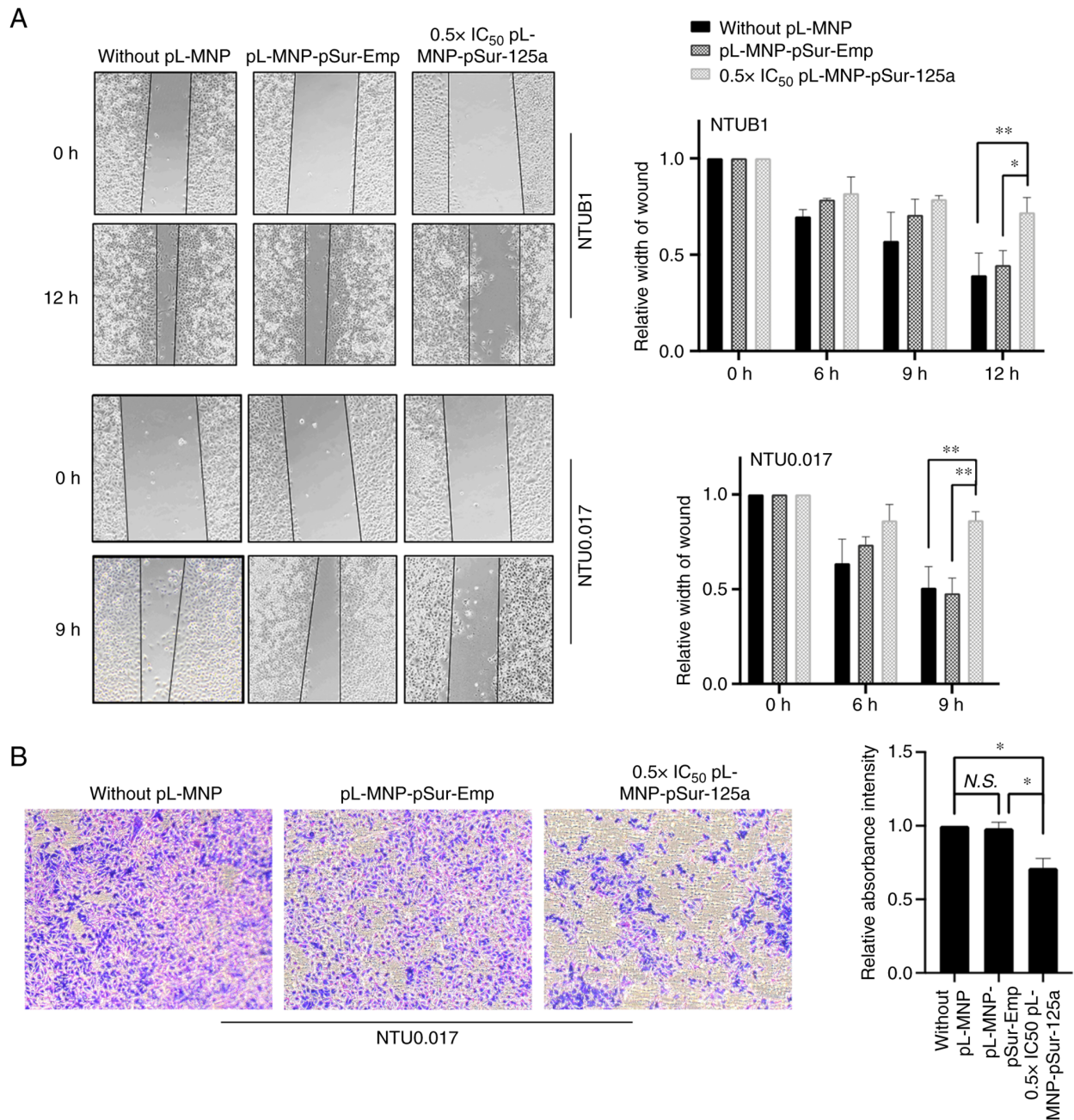| Cell line	HMEC-1	KB	KB-TAX50	NTUB1	NTU0.017
Tissue type	Microvascular endothelial	Cervical cancer	Cervical cancer	Bladder cancer	Bladder cancer
Drug resistance	N/A	-	Paclitaxel Vincristine YM155	-	Paclitaxel Vincristine YM155
ABCB1 status	Negative	Negative	Positive	Negative	Positive
pL-MNP-pSur-125a (IC_{50}, ng/μl)	>12 (unable to determine)	2.8±0.5	3.6±1.3	7.2±0.6	8.6±0.4

Figure 4. pL-MNP-pSur-125a affects the migration and invasion ability of cancer cells. (A) NTUB1 and NTU0.017 cells were treated with or without the same amount of pL-MNP-pSur-Emp and pL-MNP-pSur-125a for various durations. Rate of cell migration was determined using the wound-healing assay. (B) NTUB1 cells were treated with the same amount of pL-MNP-pSur-Emp and pL-MNP-pSur-125a for 20 h. Rate of cell invasion was determined using the Transwell invasion assay. *P<0.05 and **P<0.01.
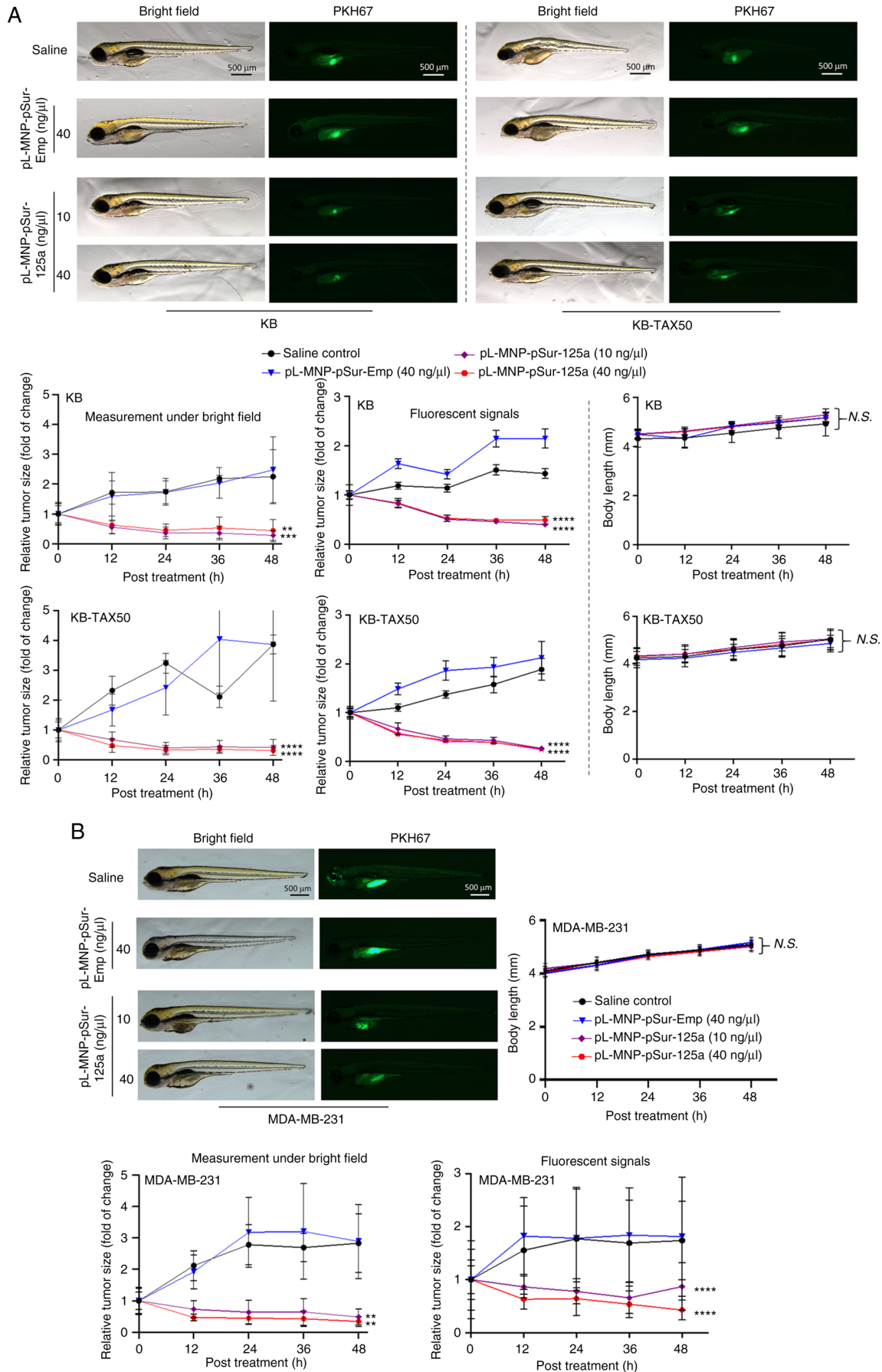
Figure 5. pL-MNP-pSur-125a suppresses tumor growth in human cancer xenograft zebrafish models. (A and B) PKH67-stained KB, KB-TAX50 and MDA-MB-231 cells were transplanted to 48 hpf zebrafish embryos (n=24). Then, zebrafish embryos were treated with saline, or the indicated concentrations of pL-MNP-pSur-Emp and pL-MNP-pSur-125a for 48 h. Tumor size and body length were measured every 12 h by immunofluorescence microscopy. **P<0.05, ***P<0.001 and ****P<0.0001 vs. pL-MNP-pSur-Emp (at the same concentration). N.S., no significance.
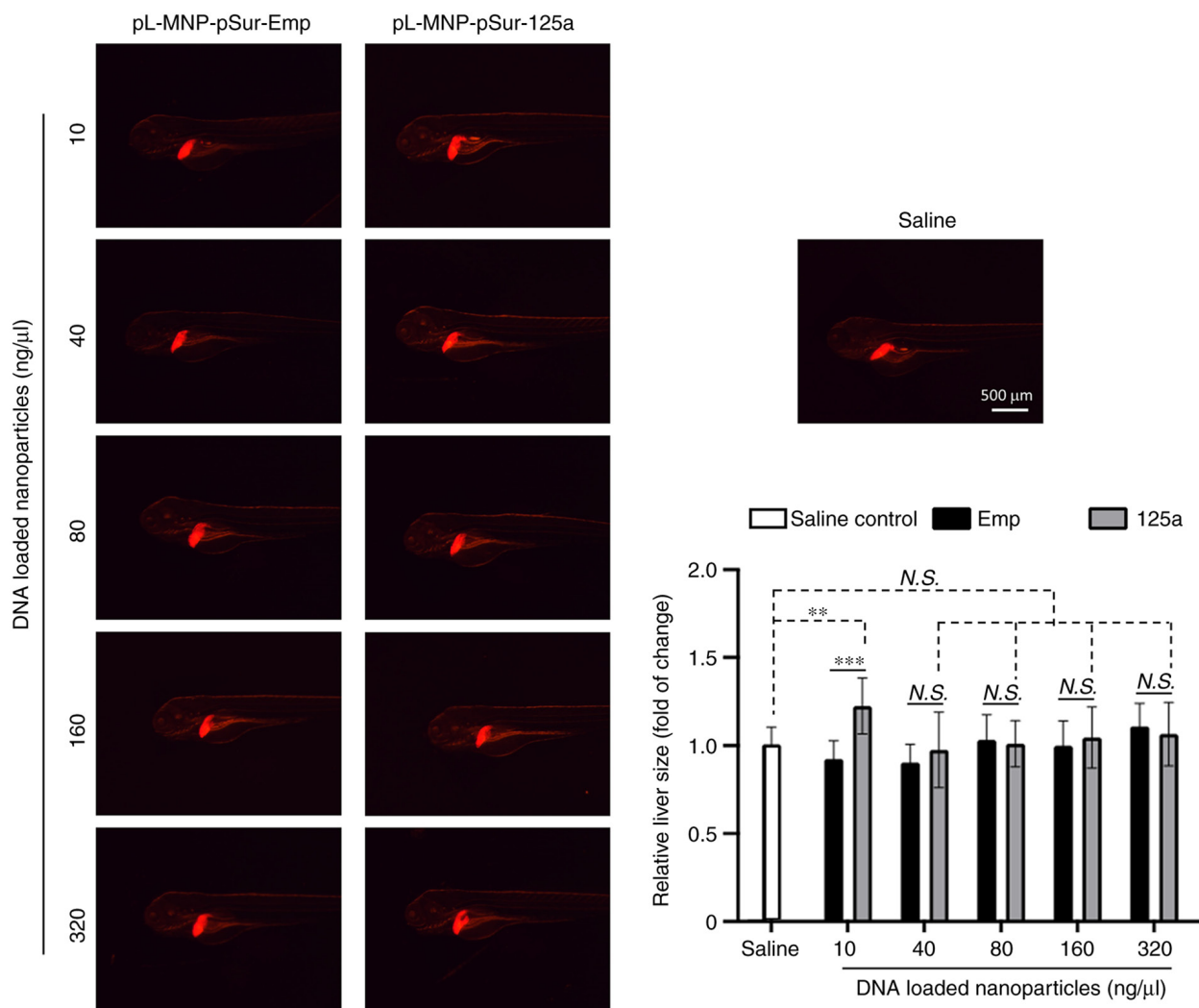
Figure 6. pL-MNP-pSur-125a does not affect the development of liver in the zebrafish model. 48 hpf transgenic zebrafish (fabp10a:mCherry) embryos were treated with saline, pL-MNP-pSur-Emp, or pL-MNP-pSur-125a for 48 h. The liver size of zebrafish embryos was observed by the immunofluorescence microscopy after 48 h post-treatment. **P<0.05 and ***P<0.001.

Upregulation of BIRC5 and SP1 promotes cancer cells migration, invasion, and tumor metastasis (51). Notably, CDH1 downregulation is frequently observed in cancer cells undergoing EMT and pL-MNP-pSur-125a increased the expression of CDH1 in KB cells (Fig. 3A). In the present study, despite the migration rate of NTUB1 and NTU0.017 cells under culturing conditions being slightly different, results of the wound-healing assay showed that pL-MNP-pSur-125a at a low cytotoxic concentration (i.e. 0.5 x IC_{50}) reduced the migration of both NTUB1and NTU0.017 cells (Fig. 4A). As NTUB1 is not suitable for use in the cell invasion assay, the potential effects of pL-MNP-pSur-125a on cell invasion were examined in NTU0.017 cells. In the present study, 0.5xIC_{50} pL-MNP-pSur-125a also decreased the invasiveness of NTU0.017 cancer cells *in vitro* (Fig. 4B).

pL-MNP-pSur-125a exhibits antitumor formation effects in vivo. The anticancer efficacy of pL-MNP-pSur-125a was assessed in zebrafish, which is a xenograft model widely used for studies of tumor development and preclinical testing of anticancer drugs (52-54). The PKH67-stained (green fluorescent) KB and KB-TAX50 cancer cells were micro-injected into the yolk sac of zebrafish embryos. As revealed in Fig. 5, pL-MNP-pSur-125a reduced the size of the KB, KB-TAX50 and MDA-MB-231 xenograft tumors in zebrafish. By contrast, neither saline nor pL-MNP-pSur-Emp showed any inhibitory effects on the growth of tumors (Fig. 5A and B). Notably, pL-MNP-pSur-125a was well-tolerated at the examined concentrations with no signs of severe toxicity in the KB, KB-TAX50 and MDA-MB-231 xenograft tumor models as the overall body length of zebrafish was similar (i.e. changes were insignificant) between the treatment and the control groups (i.e. saline and pL-MNP-pSur-Emp) (Fig. 5A and B).

The possible hepatotoxicity effect of pL-MNP-pSur-125a was also examined in zebrafish, as it is an *in vivo* model commonly used to study drug-induced liver injury (55,56). Decreased liver size is a sign of liver damage. In the present study, pL-MNP-pSur-125a did not show any negative-effects on the size of the liver at most examined concentrations (except for 10 and 640 ng/μl, with slightly increased liver size), suggesting that the use of pL-MNP-pSur-125a may not induce liver damage during the treatment (Fig. 6).
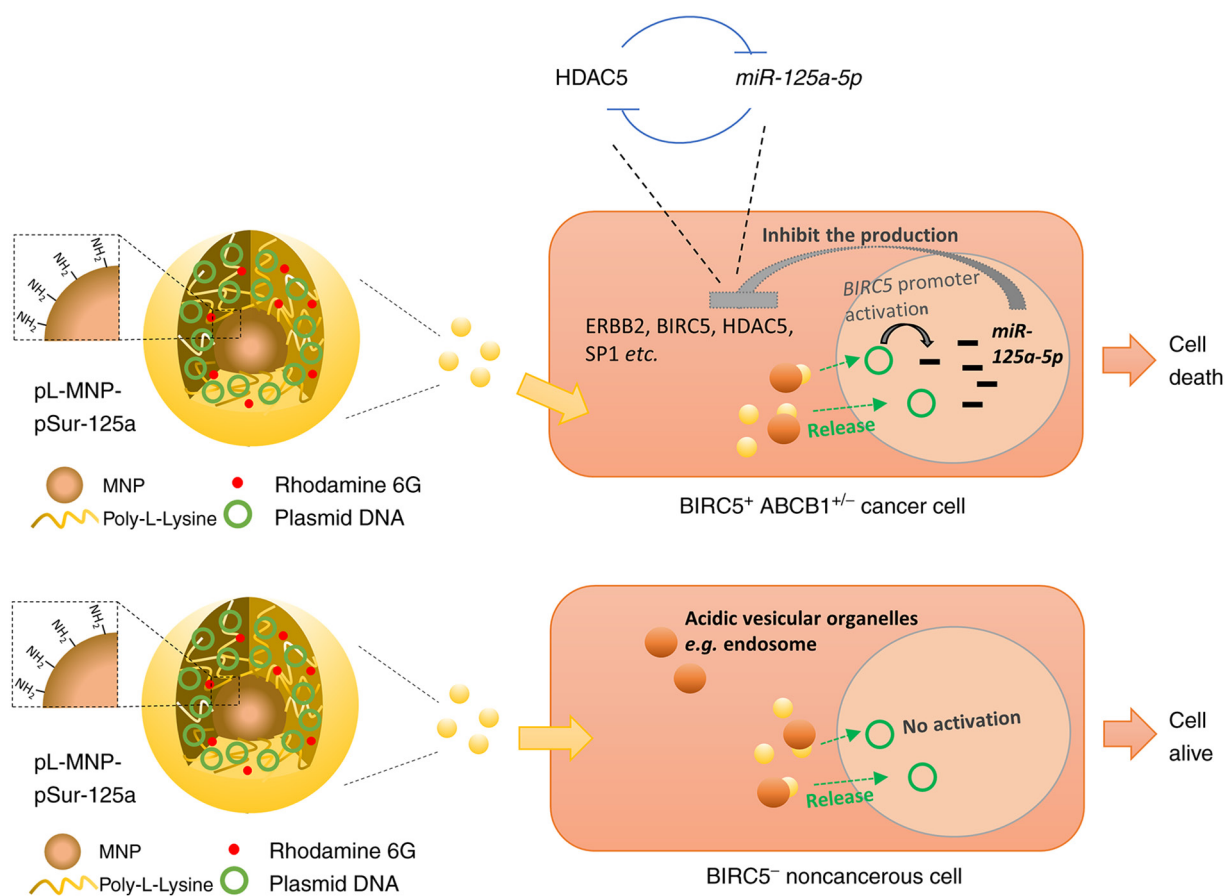
Figure 7. Structure and functions of pL-MNP-pSur-125a. Molecular and cellular effects of pL-MNP-pSur-125a in BIRC5+ cancer cells and in BIRC5- noncancerous cells.

Discussion

In the present study, pL-MNP was successfully utilized as a transfection agent and the high gene expression efficiency of DNA-loaded pL-MNP (pL-MNP-pSur-125a) in BIRC5-expressing cancer cells was demonstrated. In this DNA-carried system, DNA was adsorbed on pL-MNP by strong electrostatic interactions and it could be released from pL-MNP by protonation of the phosphate group in DNA under acidic conditions (Fig. 7). During the production of pL-MNP-pSur-125a from pL-MNP, the increased hydrodynamic diameter (from ~289 to ~327 nm) and the charge transformation (from positive to negative charge) of zeta potential indicated the successful adsorption of pSur-125a on pL-MNP. Moreover, a high degree of overlap between the two chemical elements, phosphorus and iron, in pL-MNP-pSur-125a as shown by the elemental distribution maps also suggests that pSur-125a was successfully adsorbed onto pL-MNP.

Functionally, pL-MNP-pSur-125a exhibits poly-pharmacological properties as it downregulates the expression of various cancer-related molecules (HDAC5, ERBB2, BIRC5 and SP1) and induces cell death in BIRC5+ cancer cells (Fig. 7). It was previously identified that HDAC5 negatively regulates the expression of miR-125a-5p in cancer cells (15). Notably, in the present study, it was found that miR-125a-5p negatively regulates the expression of HDAC5. Co-incubation

with the BIRC5 expression-suppressant (through the binding on the BIRC5 gene promotor region), YM155, only partially suppressed the increased-expression of miR-125a-5p in cells transfected with pSur-125a. The use of YM155 at low concentration (i.e. sublethal concentration) in the experiment may be one of the reasons behind the incomplete suppression of the increased-expression of miR-125a-5p in the pSur-125a-transfected cells. It is also possible that the increased amount of miR-125a-5p transcripts present in the pSur-125a-transfected cells was not solely caused by the BIRC5 promotor-driven miR-125a-5p expressing function of pSur-125a but also partly caused by the decreased expression of HDAC5 (induced by the pSur-125a-expressing miR-125a-5p), leading to the increased expression of the endogenous miR-125a-5p in cells (i.e. activating the endogenous feedback loop between HDAC5 and miR-125a-5p). Although the expression of the well-known anti-apoptotic molecule, B-cell lymphoma 2 (BCL2), was not examined in the pL-MNP-pSur-125a-treated cancer cells in the present study, it was demonstrated in a previous study that ectopic overexpression of miR-125a-5p decreases the expression of BCL2 in MCF7, MCF7-TamC3 and SK-BR-3 breast cancer cells (15). As BCL2 mRNA contains a putative miR-125a-5p binding site in the 3' untranslated region (position 2419-2426 of BCL2 3'UTR), it is considered that pL-MNP-pSur-125a should also downregulate the expression of BCL2 in various BIRC5+ cancer cells.

Two of the most important pharmacological features of pL-MNP-pSur-125a are the following: i) this nanodrug is designed to be activated primarily in tumors, but not in the differentiated normal tissues, as BIRC5 is highly expressed in cancer cells, but not in the differentiated normal cells, and ii) the potency of this nanodrug is not affected by the expression of the multidrug resistant protein ABCB1 in cancer cells. Drug resistance is known to be a major clinical problem in cancer treatment. Upregulation of a drug efflux transporter ABCB1 causes cancer cells to become refractory to various chemotherapeutic, targeted therapeutic and hormonal drugs such as paclitaxel (mitotic inhibitor), doxorubicin (topoisomerase inhibitor), olaparib [poly ADP-ribose polymerase inhibitor (PARPi)], and tamoxifen [selective estrogen receptor modulator (SERM)] (57-60). Besides ABCB1, upregulation of BIRC5 is also known to promote multidrug resistance in cancer cells. For example, Park *et al* demonstrated that overexpression of BIRC5 promotes vincristine (mitotic inhibitor) resistance, whereas downregulation of BIRC5 increases the sensitivity to vincristine in acute lymphoblastic leukemia cells (61). It was previously demonstrated that dysregulation of the HDAC5-BIRC5-signaling pathway contributes to the development of both estrogen independence and hormone therapy resistance in estrogen receptor-positive (ER$^+$) breast cancer cells (15). Overexpression of HDAC5 has also been shown to promote SOX9 deacetylation and nuclear translocation, contributing to tamoxifen resistance in ER$^+$ breast cancer (62). In the case of ERBB2, overexpression or hyperactivation of this EGFR family member has been demonstrated to regulate the NRF2-dependent transcriptional activation, leading to the induction of antioxidant response and drug resistance in cancer cells (63). The expression of ERBB2 and the activation of its downstream signaling pathway is also known to play an important role in the survival of ERBB2$^+$ breast cancer (i.e. the HER2-enriched subtype). On the other hand, TDO2 plays a pivotal role in regulating the immune microenvironment in tumors and overexpression of TDO2 promotes tumor immune evasion (64,65). Thus, various efforts have been made to the development of HDAC5 (e.g., LMK-235), BIRC5 (e.g., YM155, SPC3042), ERBB2 (e.g., Herceptin, Irbinitinib) and TDO2 (e.g., 680C91 and LM10) modulators/inhibitors for cancer treatment and several of them have reached clinical trials (30,31,35,45,48,66). Not to mention that the anti-ERBB2 monoclonal antibody, Herceptin, is already being used clinically in treating patients with ERBB2$^+$ (i.e. HER2$^+$) breast cancer. Given the roles of BIRC5, ERBB2, HDAC5 and TDO2 in survival of tumor cells, pL-MNP-pSur-125a is a promising nanodrug that has potential for the management of various malignancies, particularly for patients with ABCB1-related multidrug resistance after prolonged chemotherapeutic treatments. In addition, since miR-125a-5p modulates the expression of various proteins, it will be interesting to investigate in the future if pL-MNP-pSur-125a can also modulate the expression of different major histocompatibility class I molecules, in which dysregulation of these molecules is known to affect the effectiveness of anticancer immunotherapy (67).

Large-sized, DNA-loaded, nanoparticles (hydrodynamic diameter of 300-600 nm) have been revealed to mediate a higher transfection and gene expression efficiency in cells as compared with the DNA-loaded nanoparticles of smaller size (<100 nm) (68,69). However, nanoparticles with a hydrodynamic diameter of 100-400 nm, particularly for those with a diameter of less than 300 nm, have widely been considered optimal for passive tumor targeting due to the enhanced permeability and retention effect (70). In addition, it has been demonstrated that nanoparticles of 100-200 nm in size can escape from recognition by the reticuloendothelial system, which prolongs the half-life of nanoparticles in blood circulation (71). As revealed by the DLS results, the average hydrodynamic diameter of pL-MNP-pSur-125a is ~360 nm. Despite the fact that the size of pL-MNP-pSur-125a is slightly larger than 300 nm, which may hamper the efficiency of 'tumor site-penetration', several studies showed that nanoparticles with size larger than 300 nm still exhibit potent anticancer effects *in vivo*. For example, Talekar *et al* (72) demonstrated that the wild-type TP53/p53 and miR-125b co-expressing plasmid DNA-loaded hyaluronic acid-based nanoparticles, in a size range of 200-400 nm, were capable of inhibiting tumor growth and inducing apoptosis in a mouse model of lung cancer. In addition, a study showed that co-delivery of doxorubicin and the *BIRC5* shRNA-expressing plasmid DNA by using mesoporous silica nanoparticles of around 350 nm in size were potent in targeting cancer cells *in vitro* and *in vivo* (73). It has also been demonstrated that chemotherapeutic drugs loaded to iron oxide mesoporous magnetic microparticles, with an average hydrodynamic size of 765 nm, were capable of penetrating the deep tumor cell layers of the dissected breast tumor tissues in culturing conditions of oxygen, nutrient and energy gradients similar to those found *in vivo* (74). Notably, fewer large-sized nanoparticles (i.e. 200-400 nm in size) were shown to be uptaken by macrophages than those of smaller size (75). As BIRC5 was expressed in atherosclerotic macrophages, the currently developed pL-MNP-pSur-125a nanoparticles in a size range of 300-400 nm may escape from being uptaken by macrophages, thereby limiting the induction of the unwanted immune responses (76). Further *in vivo* studies (e.g., by using genetically engineered mice) are needed to determine if pL-MNP-pSur-125a, at the current size, remains functional in targeting BIRC5$^+$ tumors in a more complex tumor environment.

In conclusion, a poly-pharmacological nanoparticle pL-MNP-pSur-125a has been successfully produced and demonstrated to exert biological activity in eliminating BIRC5-expressing cancer cells, regardless of the tissue origins and the expression of the multidrug efflux pump ABCB1. PL-MNP-pSur-125a is a promising anticancer nanodrug that has the potential for the management of various malignancies, particularly for patients with ABCB1-related drug resistance after prolonged chemotherapeutic treatments.

Funding

Availability of data and materials

The datasets used and/or analyzed during the current study are available from the corresponding author on reasonable request.

Authors' contributions

Y-CC, M-CS, Y-HC, W-LH, W-CS, F-YC and CHAC conceived and designed the experiments. Y-CC, Y-HC and F-YC performed the experiments. Y-CC, Y-HC and F-YC analyzed the data. Y-CC and Y-HC confirm the authenticity of all the raw data. F-YC and CHAC wrote and proofread the paper. All authors read and approved the final manuscript.

Ethics approval and consent to participate

The animal protocol was approved (approval no. 109273) by the Institutional Animal Care and Use Committee (IACUC) of National Cheng Kung University (Tainan, Taiwan).

Patient consent for publication

Not applicable.

Competing interests

The authors declare that they have no competing interests.

References

1. Groenendijk FH and Bernards R: Drug resistance to targeted therapies: Déjà vu all over again. Mol Oncol 8: 1067-1083, 2014.
2. Xie L and Bourne PE: Developing multi-target therapeutics to fine-tune the evolutionary dynamics of the cancer ecosystem. Front Pharmacol 6: 209, 2015.
3. Antolin AA, Workman P, Mestres J and Al-Lazikani B: Polypharmacology in precision oncology: Current applications and future prospects. Curr Pharm Design 22: 6935-6945, 2016.
4. Nishida N, Mimori K, Fabbri M, Yokobori T, Sudo T, Tanaka F, Shibata K, Ishii H, Doki Y and Mori M: MicroRNA-125a-5p is an independent prognostic factor in gastric cancer and inhibits the proliferation of human gastric cancer cells in combination with trastuzumab. Clin Cancer Res 17: 2725-2733, 2011.
5. Hsieh TH, Hsu CY, Tsai CF, Long CY, Chai CY, Hou MF, Lee JN, Wu DC, Wang SC and Tsai EM: miR-125a-5p is a prognostic biomarker that targets HDAC4 to suppress breast tumorigenesis. Oncotarget 6: 494, 2014.
6. Vo DT, Karanam NK, Ding L, Saha D, Yordy JS, Giri U, Heymach JV and Story MD: miR-125a-5p functions as tumor suppressor microRNA and is a marker of locoregional recurrence and poor prognosis in head and neck cancer. Neoplasia 21: 849-862, 2019.
7. Liang Z, Pan Q, Zhang Z, Huang C, Yan Z, Zhang Y and Li J: MicroRNA-125a-5p controls the proliferation, apoptosis, migration and PTEN/MEK1/2/ERK1/2 signaling pathway in MCF-7 breast cancer cells. Mol Med Rep 20: 4507-4514, 2019.
8. Yan L, Yu MC, Gao GL, Liang HW, Zhou XY, Zhu ZT, Zhang CY, Wang YB and Chen X: MiR-125a-5p functions as a tumour suppressor in breast cancer by downregulating BAP1. J Cell Biochem 119: 8773-8783, 2018.
9. Tang L, Zhou L, Wu S, Shi X, Jiang G, Niu S and Ding D: miR-125a-5p inhibits colorectal cancer cell epithelial-mesenchymal transition, invasion and migration by targeting TAZ. Onco Targets Ther 12: 3481-3489, 2019.
10. Tong Z, Liu N, Lin L, Guo X, Yang D and Zhang Q: miR-125a-5p inhibits cell proliferation and induces apoptosis in colon cancer via targeting BCL2, BCL2L12 and MCL1. Biomed Pharmacother 75: 129-136, 2015.
11. Zhong L, Sun S, Shi J, Cao F, Han X and Chen Z: MicroRNA-125a-5p plays a role as a tumor suppressor in lung carcinoma cells by directly targeting STAT3. Tumor Biol 39: 1010428317697579, 2017.
12. Hsieh TH, Hsu CY, Tsai CF, Long CY, Wu CH, Wu DC, Lee JN, Chang WC and Tsai EM: HDAC inhibitors target HDAC5, upregulate microRNA-125a-5p, and induce apoptosis in breast cancer cells. Mol Ther 23: 656-666, 2015.
13. Xu Y, Zheng Y, Duan Y, Ma L and Nan P: MicroRNA-125a-5p targets LIM kinase 1 to inhibit cisplatin resistance of cervical cancer cells. Oncol Lett 21: 392, 2021.
14. Cao Q, Wang N, Ren L, Tian J, Yang S and Cheng H: miR-125a-5p post-transcriptionally suppresses GALNT7 to inhibit proliferation and invasion in cervical cancer cells via the EGFR/PI3K/AKT pathway. Cancer Cell Int 20: 117, 2020.
15. Huang WT, Tsai YH, Chen SH, Kuo CW, Kuo YL, Lee KT, Chen WC, Wu PC, Chuang CY, Cheng SM, et al: HDAC2 and HDAC5 up-regulations modulate survivin and miR-125a-5p expressions and promote hormone therapy resistance in estrogen receptor positive breast cancer cells. Front Pharmacol 8: 902, 2017.
16. Zhang Y, Li A, Shi J, Fang Y, Gu C, Cai J, Lin C, Zhao L and Liu S: Imbalanced LIMK1 and LIMK2 expression leads to human colorectal cancer progression and metastasis via promoting β-catenin nuclear translocation. Cell Death Dis 9: 749, 2018.
17. Cheung CH, Chen HH, Kuo CC, Chang CY, Coumar MS, Hsieh HP and Chang JY: Survivin counteracts the therapeutic effect of microtubule de-stabilizers by stabilizing tubulin polymers. Mol Cancer 8: 43, 2009.
18. Mahalaxmi I and Santhy KS: Role and hallmarks of Sp1 in promoting ovarian cancer. J Oncol Sci 4: 102-105, 2018.
19. Jiang Y, de Bruin A, Caldas H, Fangusaro J, Hayes J, Conway EM, Robinson ML and Altura RA: Essential role for survivin in early brain development. J Neurosci 25: 6962-6970, 2005.
20. Ambrosini G, Adida C and Altieri DC: A novel anti-apoptosis gene, survivin, expressed in cancer and lymphoma. Nat Med 3: 917-921, 1997.
21. Vischioni B, van der Valk P, Span SW, Kruyt FAE, Rodriguez JA and Giaccone G: Nuclear localization of survivin is a positive prognostic factor for survival in advanced non-small-cell lung cancer. Ann Oncol 15: 1654-1660, 2004.
22. Zhang L, Yan R, Zhang Q, Wang H, Kang X, Li J, Yang S, Zhang J, Liu Z and Yang X: Survivin, a key component of the Wnt/β-catenin signaling pathway, contributes to traumatic brain injury-induced adult neurogenesis in the mouse dentate gyrus. Int J Mol Med 32: 867-875, 2013.
23. Bao R, Connolly DC, Murphy M, Green J, Weinstein JK, Pisarcik DA and Hamilton TC: Activation of cancer-specific gene expression by the survivin promoter. J Natl Cancer Inst 94: 522-528, 2002.
24. Yang L, Cao Z, Li F, Post DE, Van Meir EG, Zhong H and Wood WC: Tumor-specific gene expression using the survivin promoter is further increased by hypoxia. Gene Ther 11: 1215-1223, 2004.
25. Siddharth S, Das S, Nayak A and Kundu CN: Survivin as a marker for quiescent-breast cancer stem cells-An intermediate, adherent, pre-requisite phase of breast cancer metastasis. Clin Exp Metastasis 33: 661-675, 2016.
26. Carter BZ, Qiu Y, Huang X, Diao L, Zhang N, Coombes KR, Mak DH, Konopleva M, Cortes J, Kantarjian HM, et al: Survivin is highly expressed in CD34+38-leukemic stem/progenitor cells and predicts poor clinical outcomes in AML. Blood 120: 173-180, 2012.
27. Zhang Y, Yan H, Li R, Guo Y and Zheng R: High expression of survivin predicts poor prognosis in cervical squamous cell carcinoma treated with paclitaxel and carboplatin. Medicine (Baltimore) 98: e15607, 2019.
28. Onodi F, Maherzi-Mechalikh C, Mougel A, Hamouda NB, Taboas C, Gueugnon F, Tran T, Nozach H, Marcon E, Gey A, et al: High therapeutic efficacy of a new survivin LSP-cancer vaccine containing CD4+ and CD8+ T-cell epitopes. Front Oncol 8: 517, 2018.

29. Voges Y, Michaelis M, Rothweiler F, Schaller T, Schneider C, Politt K, Mernberger M, Nist A, Stiewe T, Wass MN, *et al*: Effects of YM155 on survivin levels and viability in neuroblastoma cells with acquired drug resistance. Cell Death Dis 7: e2410, 2016.

30. Nakahara T, Kita A, Yamanaka K, Mori M, Amino N, Takeuchi M, Tominaga F, Hatakeyama S, Kinoyama I, Matsuhisa A, *et al*: YM155, a novel small-molecule survivin suppressant, induces regression of established human hormone-refractory prostate tumor xenografts. Cancer Res 67: 8014-8021, 2007.

31. Hansen JB, Fisker N, Westergaard M, Kjaerulff LS, Hansen HF, Thrue CA, Rosenbohm C, Wissenbach M, Orum H and Koch T: SPC3042: A proapoptotic survivin inhibitor. Mol Cancer Ther 7: 2736-2745, 2008.

32. Tolcher AW, Mita A, Lewis LD, Garrett CR, Till E, Daud AI, Patnaik A, Papadopoulos K, Takimoto C, Bartels P, *et al*: Phase I and pharmacokinetic study of YM155, a small-molecule inhibitor of survivin. J Clin Oncol 26: 5198-5203, 2008.

33. Cheung CHA, Sun X, Kanwar JR, Bai JZ, Cheng L and Krissansen GW: A cell-permeable dominant-negative survivin protein induces apoptosis and sensitizes prostate cancer cells to TNF-α therapy. Cancer Cell Int 10: 36, 2010.

34. Tsai SL, Chang YC, Sarvagalla S, Wang S, Coumar MS and Cheung CHA: Cloning, expression, and purification of the recombinant pro-apoptotic dominant-negative survivin T34A-C84A protein in Escherichia coli. Protein Expr Purif 160: 73-83, 2019.

35. Quispe PA, Lavecchia MJ and León IE: On the discovery of a potential survivin inhibitor combining computational tools and cytotoxicity studies. Heliyon 5: e02238, 2019.

36. Arigita C, Zuidam NJ, Crommelin DJ and Hennink WE: Association and dissociation characteristics of polymer/DNA complexes used for gene delivery. Pharm Res 16: 1534-1541, 1999.

37. Lin KY, Cheng SM, Tsai SL, Tsai JY, Lin CH and Cheung CHA: Delivery of a survivin promoter-driven antisense survivin-expressing plasmid DNA as a cancer therapeutic: A proof-of-concept study. Onco Targets Ther 9: 2601-2613, 2016.

38. Cheung CH, Lin WH, Hsu JTA, Hour TC, Yeh TK, Ko S, Lien TW, Coumar MS, Liu JF, Lai WY, *et al*: BPR1K653, a novel Aurora kinase inhibitor, exhibits potent anti-proliferative activity in MDR1 (P-gp170)-mediated multidrug-resistant cancer cells. PLoS One 6: e23485, 2011.

39. Chang YC, Kondapuram SK, Yang TH, Syed SB, Cheng SM, Lin TY, Lin YC, Coumar MS, Chang JY, Leung E and Cheung CHA: The SMAC mimetic LCL161 is a direct ABCB1/MDR1-ATPase activity modulator and BIRC5/Survivin expression down-regulator in cancer cells. Toxicol Appl Pharmacol 401: 115080, 2020.

40. Lee PC, Lee HJ, Kakadiya R, Sanjiv K, Su TL and Lee TC: Multidrug-resistant cells overexpressing P-glycoprotein are susceptible to DNA crosslinking agents due to attenuated Src/nuclear EGFR cascade-activated DNA repair activity. Oncogene 32: 1144-1154, 2013.

41. Yu HJ, Tsai TC, Hsieh TS and Chiu TY: Characterization of a newly established human bladder carcinoma cell line, NTUB1. J Formos Med Assoc 91: 608-613, 1992.

42. Leung E, Kannan N, Krissansen GW, Findlay MP and Baguley BC: MCF-7 breast cancer cells selected for tamoxifen resistance acquire new phenotypes differing in DNA content, phospho-HER2 and PAX2 expression, and rapamycin sensitivity. Cancer Biol Ther 9: 717-724, 2010.

43. Livak KJ and Schmittgen TD: Analysis of relative gene expression data using real-time quantitative PCR and the 2(-Delta Delta C(T)) method. Methods 25: 402-408, 2001.

44. Jiang G, Ren B, Xu L, Song S, Zhu C and Ye F: Survivin may enhance DNA double-strand break repair capability by up-regulating Ku70 in human KB cells. Anticancer Res 29: 223-228, 2009.

45. Cheng Q, Ling X, Haller A, Nakahara T, Yamanaka K, Kita A, Koutoku H, Takeuchi M, Brattain MG and Li F: Suppression of survivin promoter activity by YM155 involves disruption of Sp1-DNA interaction in the survivin core promoter. Int J Biochem Mol Biol 3: 179-197, 2012.

46. Al-Sharif I, Remmal A and Aboussekhra A: Eugenol triggers apoptosis in breast cancer cells through E2F1/survivin down-regulation. BMC Cancer 13: 600, 2013.

47. Meng F, Cheng R, Deng C and Zhong Z: Intracellular drug release nanosystems. Materials Today 15: 436-442, 2012.

48. de Iudicibus RC, Tomek P, Palmer BD, Tijono SM, Flanagan JU and Ching LM: Parallel discovery of selective and dual inhibitors of tryptophan dioxygenases IDO1 and TDO2 with a newly-modified enzymatic assay. Bioorg Med Chem 39: 116160, 2021.

49. Sari S, Tomek P, Leung E and Reynisson J: Discovery and characterisation of dual inhibitors of tryptophan 2,3-Dioxygenase (TDO2) and indoleamine 2,3-dioxygenase 1 (IDO1) using virtual screening. Molecules 24: 4346, 2019.

50. Gong Y, Li Y, Abdolmaleky HM, Li L and Zhou JR: Tanshinones inhibit the growth of breast cancer cells through epigenetic modification of aurora a expression and function. PLoS One 7: e33656, 2012.

51. Tai CJ, Chin-Sheng H, Kuo LJ, Wei PL, Lu HH, Chen HA, Liu TZ, Liu JJ, Liu DZ, Ho YS, *et al*: Survivin-mediated cancer cell migration through GRP78 and epithelial-mesenchymal transition (EMT) marker expression in mahlavu cells. Ann Surg Oncol 19: 336-343, 2012.

52. Al-Thani HF, Shurbaji S and Yalcin HC: Zebrafish as a model for anticancer nanomedicine studies. Pharmaceuticals (Basel) 14: 625, 2021.

53. Letrado P, de Miguel I, Lamberto I, Díez-Martínez R and Oyarzabal J: Zebrafish: Speeding up the cancer drug discovery process. Cancer Res 78: 6048-6058, 2018.

54. Hason M and Bartůněk P: Zebrafish models of cancer-new insights on modeling human cancer in a non-mammalian vertebrate. Genes (Basel) 10: 935, 2019.

55. He JH, Guo SY, Zhu F, Zhu JJ, Chen YX, Huang CJ, Gao JM, Dong QX, Xuan YX and Li CQ: A zebrafish phenotypic assay for assessing drug-induced hepatotoxicity. J Pharmacol Toxicol Methods 67: 25-32, 2013.

56. Vliegenthart ADB, Tucker CS, Pozo JD and Dear JW: Zebrafish as model organisms for studying drug-induced liver injury. Br J Clin Pharmacol 78: 1217-1227, 2014.

57. Mechetner E, Kyshtoobayeva A, Zonis S, Kim H, Stroup R, Garcia R, Parker RJ and Fruehauf JP: Levels of multidrug resistance (MDR1) P-glycoprotein expression by human breast cancer correlate with in vitro resistance to taxol and doxorubicin. Clin Cancer Res 4: 389-398, 1998.

58. Duan Z, Brakora KA and Seiden MV: Inhibition of ABCB1 (MDR1) and ABCB4 (MDR3) expression by small interfering RNA and reversal of paclitaxel resistance in human ovarian cancer cells. Mol Cancer Ther 3: 833-838, 2004.

59. Krisnamurti DGB, Louisa M, Anggraeni E and Wanandi SI: Drug efflux transporters are overexpressed in short-term tamoxifen-induced MCF7 breast cancer cells. Adv Pharmacol Sci 2016: 6702424, 2016.

60. Vaidyanathan A, Sawers L, Gannon AL, Chakravarty P, Scott AL, Bray SE, Ferguson MJ and Smith G: ABCB1 (MDR1) induction defines a common resistance mechanism in paclitaxel- and olaparib-resistant ovarian cancer cells. Br J Cancer 115: 431-441, 2016.

61. Park E, Gang EJ, Hsieh YT, Schaefer P, Chae S, Klemm L, Huantes S, Loh M, Conway EM, Kang ES, *et al*: Targeting survivin overcomes drug resistance in acute lymphoblastic leukemia. Blood 118: 2191-2199, 2011.

62. Xue Y, Lian W, Zhi J, Yang W, Li Q, Guo X, Gao J, Qu H, Lin W, Li Z, *et al*: HDAC5-mediated deacetylation and nuclear localisation of SOX9 is critical for tamoxifen resistance in breast cancer. Br J Cancer 121: 1039-1049, 2019.

63. Kang HJ, Yi YW, Hong YB, Kim HJ, Jang YJ, Seong YS and Bae I: HER2 confers drug resistance of human breast cancer cells through activation of NRF2 by direct interaction. Sci Rep 4: 7201, 2014.

64. Liu Q, Zhai J, Kong X, Wang X, Wang Z, Fang Y and Wang J: Comprehensive analysis of the expressionand prognosis for TDO2 in breast cancer. Mol Ther Oncolytics 17: 153-168, 2020.

65. Miyazaki T, Chung S, Sakai H, Ohata H, Obata Y, Shiokawa D, Mizoguchi Y, Kubo T, Ichikawa H, Taniguchi H, *et al*: Stemness and immune evasion conferred by the TDO2-AHR pathway are associated with liver metastasis of colon cancer. Cancer Sci 113: 170-181, 2022.

66. Wanek J, Gaisberger M, Beyreis M, Mayr C, Helm K, Primavesi F, Jäger T, Fazio PD, Jakab M, Wagner A, *et al*: Pharmacological inhibition of class IIA HDACs by LMK-235 in pancreatic neuroendocrine tumor cells. Int J Mol Sci 19: 3128, 2018.

67. Dhatchinamoorthy K, Colbert JD and Rock KL: Cancer immune evasion through loss of MHC class I antigen presentation. Front Immunol 12: 636568, 2021.

68. Ogris M, Steinlein P, Kursa M, Mechtler K, Kircheis R and Wagner E: The size of DNA/transferrin-PEI complexes is an important factor for gene expression in cultured cells. Gene Ther 5: 1425-1433, 1998.

69. Ogris M, Steinlein P, Carotta S, Brunner S and Wagner E: DNA/polyethylenimine transfection particles: Influence of ligands, polymer size, and PEGylation on internalization and gene expression. AAPS PharmSci 3: E21, 2001.
70. Kalyane D, Raval N, Maheshwari R, Tambe V, Kalia K and Tekade RK: Employment of enhanced permeability and retention effect (EPR): Nanoparticle-based precision tools for targeting of therapeutic and diagnostic agent in cancer. Mater Sci Eng C Mater Biol Appl 98: 1252-1276, 2019.
71. Kulkarni SA and Feng SS: Effects of particle size and surface modification on cellular uptake and biodistribution of polymeric nanoparticles for drug delivery. Pharm Res 30: 2512-2522, 2013.
72. Talekar M, Trivedi M, Shah P, Ouyang Q, Oka A, Gandham S and Amiji MM: Combination wt-p53 and MicroRNA-125b transfection in a genetically engineered lung cancer model using dual CD44/EGFR-targeting nanoparticles. Mol Ther 24: 759-769, 2016.
73. Li Z, Zhang L, Tang C and Yin C: Co-delivery of doxorubicin and survivin shRNA-expressing plasmid via microenvironment-responsive dendritic mesoporous silica nanoparticles for synergistic cancer therapy. Pharm Res 34: 2829-2841, 2017.
74. El-Boubbou K, Ali R, Al-Zahrani H, Trivilegio T, Alanazi AH, Khan AL, Boudjelal M and AlKushi A: Preparation of iron oxide mesoporous magnetic microparticles as novel multidrug carriers for synergistic anticancer therapy and deep tumor penetration. Sci Rep 9: 9481, 2019.
75. Behzadi S, Serpooshan V, Tao W, Hamaly MA, Alkawareek MY, Dreaden EC, Brown D, Alkilany AM, Farokhzad OC and Mahmoudi M: Cellular uptake of nanoparticles: Journey inside the cell. Chem Soc Rev 46: 4218-4244, 2017.
76. Blanc-Brude OP, Teissier E, Castier Y, Lesèche G, Bijnens AP, Daemen M, Staels B, Mallat Z and Tedgui A: IAP survivin regulates atherosclerotic macrophage survival. Arterioscler Thromb Vasc Biol 27: 901-907, 2007.